Engineered biochar as a tool for nitrogen pollutants removal: preparation, characterization and sorption study

Eva Viglašová[a,b,c,*], Michal Galamboš[a], David Diviš[d], Zuzana Danková[e,f], Martin Daňo[b], Lukáš Krivosudský[d], Christian L. Lengauer[g], Marek Matik[f], Jaroslav Briančin[f], Gerhard Soja[c,h]

[a]*Department of Nuclear Chemistry, Faculty of Natural Sciences, Comenius University in Bratislava, Ilkovičova 6, 842 15 Bratislava, Slovakia,*
Tel. (+421) 2 602 96 351; Fax: (+421) 2 602 96 273; emails: eva.viglasova@uniba.sk (E. Viglašová), michal.galambos@uniba.sk (M. Galamboš)
[b]*Department of Nuclear Chemistry, Faculty of Nuclear Sciences and Physical Engineering, Czech Technical University in Prague,*
Břehová 7, 115 19 Prague, Czech Republic, Tel. (+420) 22435 8230; Fax: (+420) 2 2231 7626; emails: eva.viglasova@uniba.sk (E. Viglašová);
martin.dano@fjfi.cvut.cz (M. Daňo)
[c]*Energy Department, Environmental Resources and Technologies, Austrian Institute of Technology GmbH, Konrad-Lorenz-Straße 24, 3430 Tulln,*
Austria, Tel. (+43) 1 47654 89362; Fax: (+43) 505 50-3452; emails: eva.viglasova@uniba.sk (E. Viglašová), Gerhard.Soja@ait.ac.at (G. Soja)
[d]*Department of Inorganic Chemistry, Faculty of Natural Sciences, Comenius University in Bratislava, Ilkovičova 6, 842 15 Bratislava,*
Slovakia, emails: david.divis7@icloud.com (D. Diviš), lukas.krivosudsky@uniba.sk (L. Krivosudský)
[e]*Regional Center Kosice, Geological state Institute of Dionyz Stur, Jesenského 8, 040 01 Košice, Slovakia,*
email: zuzana.dankova@geology.sk (Z. Danková)
[f]*Institute of Geotechnics, Slovak Academy of Sciences, Watsonova 45, 040 01 Košice, Slovakia, Tel. (+421) 55 7 922 624,*
Fax: (+421) 55 7 922 624; emails: matik@saske.sk (M. Matik), briancin@saske.sk (J. Briančin)
[g]*Department of Mineralogy and Crystallography, University of Vienna, Althanstraße 14, 1090 Vienna, Austria, Tel. (+43) 1 4277 53243;*
Fax: (+43) 1 4277 853243; email: christian.lengauer@univie.ac.at (C.L. Lengauer)
[h]*University for Natural Resources and Life Sciences Vienna, Institute for Chemical and Energy Engineering, Muthgasse 107,*
1190 Vienna, Austria, Tel. (+43) 1 47654 89362; email: Gerhard.Soja@boku.ac.at (G. Soja)

ABSTRACT

In this study, engineered (chemically modified) biochars (pyrolyzed bamboo biomass) were used for the removal of oxidized and reduced nitrogen species from an aqueous solution. The physico-chemical properties of the prepared materials, such as surface functional groups, elemental composition, morphology, and specific surface area were investigated. The biochar surfaces were covered with Mg and Fe particles. The particles containing Mg and Fe species were observed in the form of nano-flakes within the biochar matrix. The efficiency of nitrate and ammonium removal was examined by sorption studies. The experimental data were fitted with sorption isotherms (Langmuir, Freundlich, and Dubinin–Raduskievich) and with kinetic models. The obtained data presented a higher sorption capacity for nitrate removal in the case of the engineered Fe-biochar and the engineered Mg-biochar compared to unmodified bamboo-based biochar. The maximum sorption capacity of modified samples decreased in the order Fe-biochar (Q_e = 10.35 mg g^{-1}), Mg-biochar (Q_e = 9.13 mg g^{-1}), and the lowest capacity was found in the unmodified biochar (Q_e = 4.41 mg g^{-1}). In the case of ammonium removal, unmodified biochar with maximum sorption capacity (Q_e = 12.60 mg g^{-1}), was more efficient than Fe-(Q_e = 5.66 mg g^{-1}), and Mg-engineered biochars (Q_e = 3.23 mg g^{-1}). The pseudo-second-order kinetic model and Langmuir isotherm model proved to be the most appropriate for the experimental sorption data. In addition, engineered Fe-biochar presented magnetic properties due to the presence of Fe$_2$O$_3$ and therefore, may be easily separated from the reaction mixtures.

Keywords: Biochar; Modification; Characterization; Sorption; N-pollutant

* Corresponding author.

1. Introduction

Groundwater plays a crucial role as a source of drinking water in rural communities and urban areas throughout the world. Unfortunately, industrial, and agricultural activities have increased the formation of inorganic pollutants and other contaminants, which has raised public concern about the quality of groundwater [1]. Several sorbents (naturally occurring biomass-based sorbents, agricultural, or industrial wastes carbon-based materials, ion exchange resins, and other synthetic organic and inorganic compounds) have been investigated to remove nitrogen-pollutants from groundwater, as well as when they are present in anionic forms such as nitrates [1–3]. The conventional processes used for the elimination of nitrogen-pollutants from water are ion exchange, reverse osmosis, electro-dialysis [3], and capacitive deionization [4]. Nitrogen species, as products of biological processes in soil and groundwater, may become pollutants if threshold values are exceeded. The existence of nitrate in soils is related to the excess use of nitrogenous fertilizers in agricultural regions. Following heavy rainfall or irrigation, these nitrates can leach into groundwater and contaminate drinking water resources [5]. Nitrogen occurs in water in compounds at various oxidation states and is either inorganically bound (nitrites, nitrates, and ammonium) or bound in organic compounds. Among the different nitrogen oxidation states, –III, +III, and +V have significant importance for environmental behavior and industrial applications. Highly relevant nitrogen species in environment are nitrate (NO_3^-) and ammonium (NH_4^+). High concentrations of nitrogen pollutants in drinking water may cause health problems, such as blue-baby syndrome or methemoglobinemia in infants, as well as stomach cancer in adults, despite the fact that nitrogen is an essential component for organism growth [1,3,4,6]. According to the World Health Organization, the safe limit of nitrate concentration in drinking water is 50 mg L^{-1}. Typical domestic wastewater contains 20–35 mg L^{-1} of total nitrogen, while ammonium (NH_4^+) is accounted for 70%–82%, and nitrate (NO_3^-) and nitrite (NO_2^-) present in a negligible quantity [4].

Biochar, as a black, carbon-rich, porous material, is developed by pyrolysis of organic biomass under oxygen-limited conditions. Due to its beneficial properties, such as easy preparation, eco-friendly, low cost, thermal, and mechanical stability, as well as a wide range of available input materials, biochar has attracted increasing attention [7–10]. The wide range of biochar application includes carbon sequestration, greenhouse gas emission reduction, land remediation, contaminant immobilization, and soil improvement [11–13]. It causes the reduction of the trace elements bioavailability, increase organic matter content of composting feedstock, increases nutrient retention. Also improves homogeneity of the mixture, increases water holding capacity, adjusts C:N ratio of compost, raises the temperature, increases microbial activities, increases buffers soil pH, reduces the concentration of exchangeable aluminum, modifies water retention, etc. [14,15]. The chemical and physical properties of biochar mainly depend on the type of input biomass, prepared feedstock, and pyrolysis conditions (e.g., residence time, temperature, heating rate, and reactor type) [16]. Among the many types of biomass, bamboo biomass as a feedstock has a lot of advantages, for example, fast growth, high porosity, a content of carbon, or high strength-weight ratio [17].

In addition to extensive scientific work on the use of pure biochar for environmental issues, several methods have also been developed to modify biochar in order to achieve novel structures or surface properties and to enhance its remediation efficacy and environmental benefits. Development of inexpensive but efficient adsorbents originating from various waste materials could be a promising alternative to the expensive conventional adsorbents [11,18–20]. The modification methods available which have been investigated could be divided into four main categories, that is, chemical and physical modifications, impregnation with mineral oxides, and magnetic modifications [11]. The consequences of modifications are mainly related to the changes in surface properties (including surface area, distribution, and charge), functional groups and the volume of the pores. Biochar's surface is usually negatively charged, resulting in a relatively low sorption capacity of anionic contaminants [21,22]. Based on these facts, engineered biochars—produced by application-oriented, outcome-based modification, or synthesis—are developed as innovative sorbents for the improvement of the environmental quality of contaminated regions, and to decrease the eco-toxic effects of anionic pollutants [2,7,10,11,19,23].

The main objective of this research was to enhance remediation properties and environmental aspects of engineered biochar with an obvious impact towards favorable sorption characteristics for nitrogen pollutants removal.

2. Materials and methods

2.1. Biochar preparation

All chemicals used during the experiments were of analytical grade quality. The magnesium chloride hexahydrate, $MgCl_2 \cdot 6H_2O$, and iron(III) chloride hexahydrate, $FeCl_3 \cdot 6H_2O$, were purchased from Fisher Scientific (Massachusetts, USA) and used without modification. All chemical solutions were prepared using deionized (DI) water <0.4 μS cm^{-1}, which was also used to rinse and wash the samples. All reagents used during experiments were of analytical purity.

Agricultural bamboo waste from greenway golden bamboo (*Phyllostachys viridiglaucescens*) was used as a biomass feedstock for unmodified biochar (BC-A) and modified samples Mg-biochar (BC-B), and Fe-biochar (BC-C).

Prior to using the bamboo for preparation of the raw or modified biochar samples, it was crushed and chopped into a particle size of 2 cm × 2 cm × 2 cm by a home mixer, washed several times with DI water to remove impurities and oven dried at 60°C for 5 h. Sorption studies were performed with the modeled solutions of nitrogen compounds, by $NaNO_3$ and NH_4Cl from Sigma-Aldrich (Customer Service Bratislava Slovakia).

2.2. Engineered biochar preparation

The feedstock of bamboo biomass for biochar preparation was pyrolyzed at 460°C at a residence time of 2 h in a rotary furnace. In order to ensure an oxygen-free environment and uniform heating conditions, nitrogen (N_2) was used as a flush gas. After the pyrolysis, the biochar samples were ground and sieved into a particle size of 0.5–1 mm. The material was rinsed several times with DI water, oven-dried at 80°C for 24 h and then stored at 22°C in polypropylene boxes for sorption and characterization experiments.

The engineered Mg-biochar was prepared from a mixture containing magnesium chloride hexahydrate, which was prepared by dissolving 40 g of $MgCl_2 \cdot 6H_2O$ in 60 mL of DI water and 150 g bamboo biomass. The biomass was immersed into the prepared $MgCl_2$ solution and stirred for 2 h. The mixture was then oven-dried at 80°C/24 h and afterwards pyrolyzed at 460°C/2 h. In order to ensure an oxygen-free environment and uniform heating conditions, nitrogen was used as a flush gas. The engineered Mg-biochar (sample BC-B) that was prepared by pyrolysis was gently ground and sieved into a particle size of 0.5–1 mm. In addition, the sample was rinsed several times by DI water, oven-dried at 80°C and stored at 22°C in polypropylene boxes for sorption and characterization experiments. The engineered Fe-biochar (sample BC-C) was prepared in the same manner as engineered Mg-biochar, however, instead of magnesium chloride hexahydrate, it contained a solution of iron(III) chloride hexahydrate (40 g of $FeCl_3 \cdot 6H_2O$ in 60 mL of H_2O).

2.3. Biochar characterization

Physico-chemical characterizations were performed for all prepared materials. The morphology of the surface was examined by the field-emission scanning electron microscope (FE-SEM) of type TESCAN MIRA 3 (Oxford Instruments, Abingdon, UK), equipped with an energy dispersive X-ray (EDX) detector.

The change in functional groups of materials was analyzed by FTIR spectroscopy on a Bruker VERTEX 70 instrument (Massachusetts, USA) by attenuated total reflection method in the range of 100–4,000 cm^{-1}.

Elemental analysis of carbon, hydrogen, nitrogen, and sulfur was performed using the elemental analyzer Vario MACRO cube (Elementary Analysensysteme GmbH, Germany), which was equipped with a thermal conductivity detector. The combustion tube was set up at 1,150°C and the reduction tube at 850°C. Sulfanilamide (C = 41.81%, N = 16.26%, H = 4.65%, S = 18.62%; wt%) was used as a carbon, hydrogen, nitrogen and sulphur analysis (CHNS) standard.

Thermogravimetric analysis was performed on a Mettler SDTA851e (Ohio, USA) from 25°C to 800°C at a rate of 5°C/min under a helium atmosphere (Messer 6.0, Bratislava, Slovakia) at a flow rate of 25 mL min^{-1}.

The textural properties of the studied samples were determined from the sorption and desorption isotherms by the method of physical sorption of nitrogen at –196°C measured with the NOVA 1200e Surface Area and Pore Size Analyzer (Quantachrome Instruments, USA). First, the samples were degassed at 350°C in a vacuum oven under a pressure lower than 2 Pa for 16 h. The measured data were processed by the BET (Brunauer–Emmet–Teller) isotherm in the range of relative pressure of 0.05–0.2 in order to obtain the value of specific surface area (S_{BET}) [24]. The values of external surface (S_t) and volume of micropores (V_{micro}) were calculated from the t-plot method using the Harkins–Jura standard isotherm [25]. The value of total pore volume (V_{tot}) was estimated from the maximum adsorption at relative pressure close to saturation pressure. The pore size distribution was obtained from the adsorption/desorption isotherm using the BJH (Barrett–Joyner–Halenda) method [26].

2.4. Batch sorption experiment

The sorption properties of biochar samples were studied using the batch equilibrium method. The sorbent batch was placed into test tubes with a solution containing sorbate with an exact concentration. The reagents were placed in sealed bottles and agitated in a laboratory shaker. Experimental conditions of sorption experiments for NO_3^- and NH_4^+ sorption onto BC: ratio biochar-solution [m:V] = [1:30] (units used in experiments: g:mL), C_0 = 5–400 mg L^{-1}, reaction time 24 h, 25°C ± 1°C. To keep the natural character of the modified biochars, pH was not adjusted. All experiments were performed in triplicates.

The influence of contact time on sorption was also investigated. A series of solutions (C_0 = 200 mg L^{-1}) with the required amount of material [m:V] = [1:30] (units used in the experiments: g:mL) was prepared. The mixtures were then shaken in time intervals from 5 min to 24 h with an agitation speed of 120 rpm at 25°C ± 1°C, and followed as well by solid-phase separation through centrifugation (10 min, 4,000 rpm). The solutions were filtered by a millex-GP syringe filter unit with a pore size of 0.22 μm. The concentration of un-sorbed NO_3^- was determined in supernatants immediately by the Griess spectrophotometric method. The NH_4^+ was determined by the Berthelot spectrophotometric method by UV Spectrophotometer (EnSpire Multimode Plate Reader). The amount of nitrate/ammonia absorbed per unit weight of sorbent was calculated by the difference of the sorbate concentrations.

2.4.1. Calculations

The amount of nitrate sorbated per unit weight of sorbent was calculated according to Eq. (1):

$$q_e = \frac{(C_0 - C_e)V}{m} \tag{1}$$

where q_e is the sorption capacity of biochar (mg g^{-1}), C_0 and C_e are the initial and equilibrated nitrate concentrations (mg L^{-1}) respectively, V is the volume of the aqueous solution (mL), and m is the mass of materials (g).

The equilibrium sorption isotherm expresses the mathematical relationship between the quantity of sorbate and equilibrium concentration of sorbate remaining in the solution at a constant temperature.

The Langmuir isotherm model [27] is a theoretical model for monolayer sorption:

$$C_S = \frac{C_{Smax} \times b \times C_{eq}}{\left(1 + b \times C_{eq}\right)} \tag{2}$$

where C_S is the sorption capacity (mol g^{-1}), C_{Smax} is the maximum of the sorption capacity corresponding to sites saturation (mol g^{-1}), C_{eq} is equilibrium concentration (mol L^{-1}), and b is the ratio of sorption/desorption rates.

The Freundlich isotherm model is the earliest known relationship describing the non-ideal and reversible sorption, not restricted the formation of monolayer [28]:

$$q_e = K_F C_{eq}^{\frac{1}{n}} \tag{3}$$

where C_{eq} is equilibrium concentration (mg L^{-1}), q_e is the amount of sorbate in the sorbent at equilibrium (mg g^{-1}), K_F is Freundlich isotherm constant (mg g^{-1}) (L g^{-1})^n and n related to sorption capacity.

The Dubinin–Rudshkevich isotherm model is an empirical model that was initially conceived for the sorption of subcritical vapors onto microspore solids following a pore-filling mechanism. It is generally applied to express the sorption mechanism [29,30].

$$q_e = (q_s) \exp(-K_{ad} \varepsilon^2) \tag{4}$$

where q_e is the amount of sorbate in the sorbent at equilibrium (mg g^{-1}), q_s is theoretical isotherm saturation capacity (mg g^{-1}), ε is the Dubinin–Radushkevich isotherm constant and K_{ad} is the Dubinin–Radushkevich isotherm constant (mol^2 kJ^{-2}).

Several models can be used to describe the sorption rate of a solute onto a sorbent, but the most commonly used are the pseudo-first-order model by Lagergren [31] based on solid capacity and the pseudo-second one by Ho and McKay [32] based on solid-phase sorption, respectively.

A kinetic model for sorption analysis is the pseudo-first-order rate expression of Lagergren in the form:

$$\frac{dq_t}{dt} = k_1 (q_e - q_t) \tag{5}$$

Integrating this for the boundary conditions $t = 0$ to $t = t$ and $q_t = 0$ to $q_t = q_{t'}$ Eq. (5) may be rearranged for linearized data plotting as shown by Eq. (6):

$$\log(q_e - q_t) = \log(q_e) - \frac{k_1}{2,303} \tag{6}$$

where k_1 the rate constant of pseudo-first-order sorption (1 min^{-1}), q_e the amount of solute sorbed at equilibrium (mg g^{-1}) and q_t amount of solute sorbed on the surface of the sorbent at any time t (mg g^{-1}).

For the pseudo-second-order rate, it is assumed that the sorption capacity is proportional to the number of active sites occupied on the sorbent, then the kinetic rate law can be rewritten as follows:

$$\frac{dq_t}{dt} = k_2 (q_e - q_t)^2 \tag{7}$$

where k_2 the rate constant of pseudo-second-order sorption (g mg^{-1} min^{-1}), q_e the amount of solute sorbed at equilibrium (mg g^{-1}), and q_t amount of solute sorbed on the surface of the sorbent at any time t (mg g^{-1}).

The curves of the sorption studies and isotherms were obtained by SigmaPlot 12.5, (Systat Software GmbH, D-40699 Erkrath).

3. Results and discussion

3.1. Characterization of biochar samples

The slow pyrolysis method was successfully used for preparation of BC-A (unmodified biochar), BC-B (engineered Mg-biochar), and BC-C (engineered Fe-biochar) samples.

The product yield of pyrolysis materials was about 50% of initial dry feedstock weight.

3.1.1. CHNS analysis

Biochar properties such as physical, chemical, and mechanical strongly depend on conditions of the preparation process. Results are obtained by engineering biochar, which is simultaneously optimized for carbon sequestration, nutrient storage, water-holding capacity, and sorption [33]. The International Biochar Initiative has graded biochar into three basic classes based on carbon content [34]:

- Class 1 biochar (contains 60% of carbon or more),
- Class 2 biochar (between 30% and 60% of carbon),
- Class 3 biochar (between 10% and 30% of carbon).

The high content of carbon is explained by the fact that biochar is prepared from plant biomass. Unmodified biochar (BC-A) belongs to Class 1, whereas the engineered biochars BC-B and BC-C are Class 2 materials. The lower content of carbon in the engineered biochars is naturally related to the sorption of Mg and Fe species on the biochar's surface, which caused a decrease in carbon concentration.

3.1.2. Low temperature nitrogen sorption analysis

Detailed analyses of sorption isotherms were performed to compare the textural properties of the studied materials and are illustrated in Fig. 1. The volume of the sorbed gas increased moderately and almost linearly for the BC-A sample in the entire range of relative pressure. The desorption isotherm presented an almost equal volume of desorbed gas in the entire range of relative pressure, and an opened hysteresis loop was observed. In this case, the studied biochar sample is probably macroporous. The BC-C sample presented a very low value of sorbed/desorbed gas in the wide range of relative pressure, only a slight increase of sorbed gas volume was observed for the final section of the isotherm. The sorption and desorption branches of BC-B isotherm were horizontal in the wide range of relative pressure and almost parallel. This isotherm is also typical for slit-shaped pores, and the first part of the isotherm indicates the presence of micropores. The so-called forced closure of the hysteresis loop at relative pressure $p/p_0 \sim 0.45$ was not observed. This phenomenon can be connected to the specific interaction between the diameter and character of pores (size, eventual type, and charge of surface ions) and nitrogen molecule with its quadrupole effect [35]. This sample showed the highest sorbed gas volume in comparison with the BC-A and BC-C samples.

The measured data from the sorption isotherm were processed by BET isotherm to calculate the value of the specific surface area (Table 2). The engineered Mg-biochar (BC-B) presented a higher volume of sorbed gas at low relative pressures (Fig. 1), which also corresponded with its higher specific surface area in comparison with the BC-A or BC-C biochars, as well as a higher total pore volume.

The analysis of BC-A unmodified biochar by the low temperature nitrogen sorption method had required a much higher sample dose than was possible for the available apparatus, therefore, the measured data were not sufficient
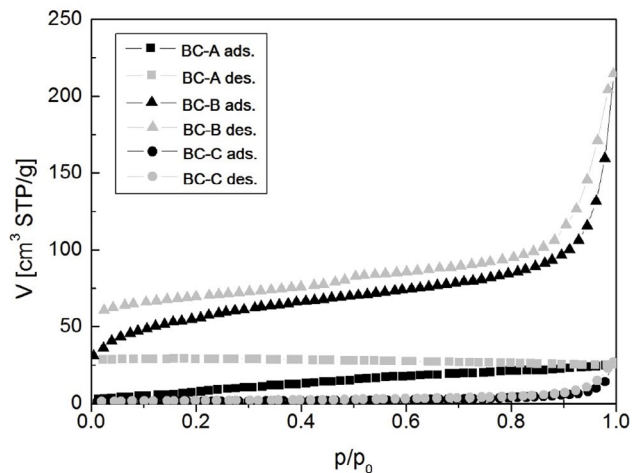
Fig. 1. Low temperature nitrogen sorption and desorption isotherms of biochars BC-A, BC-B, and BC-C (Table 1).

Table 1
Content (%) of elements by CHNS analysis. unmodified biochar (BC-A), engineered Mg-biochar (BC-B), and engineered Fe-biochar (BC-C)

	C	H	N	S
BC-A	80.97	3.89	0.52	0.43
BC-B	47.46	3.01	0.38	0.19
BC-C	44.75	2.05	0.18	0.33

to obtain a satisfactory correlation for the applied BET method. This fact corresponded with the higher difference between specific surface area and external surface area as well. According to the morphology observation described below, the prepared bamboo-based biochar displayed a well-developed porosity containing large pores (macropores). Therefore, the nitrogen sorption method was not very convenient for their characterization, however, it was still sufficient for comparison of the textural changes after biochar treatment.

Table 2
Textural parameters of studied biochars: S_{BET}, value of specific surface area; V_{tot}, total pore volume; S_t, external surface area; V_{micro}, volume of micropores

	S_{BET} (m²/g)	V_{tot} (cm³/g)	S_t (m²/g)	V_{micro} (cm³/g)
BC-A	28	0.0395	59	0.0000
BC-B	156	0.1382	103	0.0195
BC-C	5.4	0.0418	3.0	0.0011

The BC-C engineered Fe-biochar showed a very small volume of sorbed gas across the wide range of relative pressures, which was also related to the low value of external surface area. The negative intercept was obtained by applying the BET isotherm, therefore, the indicated value of the specific surface area is not of a physical meaning and should not be regarded for this sample.

Considering the shape of the BC-A desorption isotherm, the pore size distribution curves for all studied samples were obtained from their sorption isotherms (Fig. 2a). A narrower distribution of mesopores, ranging between 12 and 34 nm in diameter and continuing with a broad distribution in the range of large mesopores and macropores, could be observed for the BC-A sample. When comparing the results obtained from the nitrogen sorption measurement and scanning electron microscopy, this sample may be considered mainly macroporous. The samples BC-B and BC-C presented a wide distribution of mesopores from 10 nm up to macropores. To study the porosity of these samples in more detail, the distribution curves obtained from the desorption isotherms (excluding the effect of capillary condensation in mesopores) were compared (Fig. 2b).

The differential distribution curves of pore size (Fig. 2b) for the engineered biochars BC-B and BC-C, calculated from the desorption isotherms, showed a significant peak at $R_p = 1.9$ nm. This corresponds with the hysteresis loop closure on the desorption isotherm and does not correspond to the real pores.

The engineered biochars BC-B and BC-C exhibit a broader distribution in the region of larger mesopores and macropores (approx. 10–100 nm), so they also partially reach the macrosphere region that corresponds to the shape of their sorption isotherms.
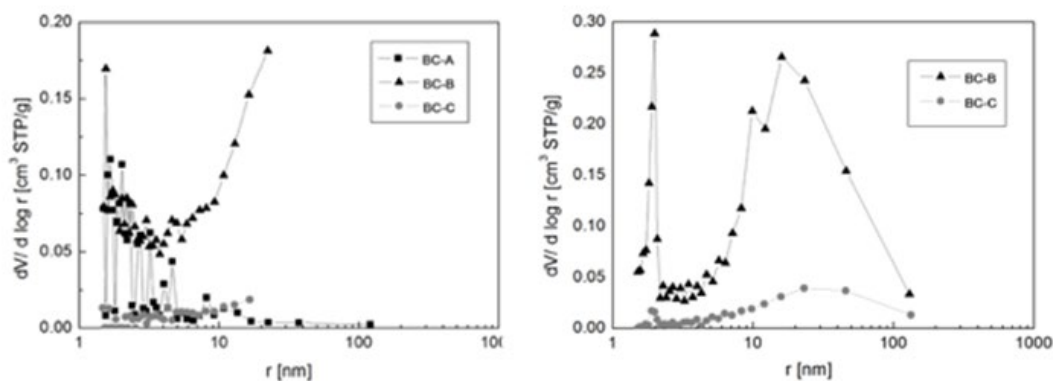

Fig. 2. (a) Differential pore size distribution curves of the analysed biochar samples determined from the sorption isotherm by BJH method. (b) Differential pore size distribution curves of the BC-B and BC-C samples determined from the desorption isotherm by BJH method.

The engineered Mg-biochar BC-B shows two more significant maxima at 19.8 and 32 nm, and the engineered Fe-biochar BC-C maxima is about 46 nm (the upper limit for mesopores).

3.1.3. Scanning electron microscope analysis, energy dispersive X-ray analysis

To investigate the surface properties (or morphology) of the engineered Mg-biochar and engineered Fe-biochar, SEM observations were used, followed by EDX/SEM examinations. The SEM images of the prepared biochar samples BC-A, BC-B, and BC-C at a final reactor temperature 460°C are shown in Fig. 3.

The unmodified biochar BC-A developed high porosity, presenting longitudinal pores (Fig. 3a) that corresponded well with the results obtained from the low temperature nitrogen sorption measurements.

The surface of the BC-B (Fig. 3c) and BC-C (Fig. 3e) engineered biochars appeared to be rougher compared with the raw bamboo feedstock (Fig. 3b). The particles containing Mg (Figs. 3c and d) and Fe (Figs. 3e and f) species were observed in the form of nanoflakes within the biochar matrix. They were distributed across the surface of the biochar (Figs. 3c–f), but did not completely cover the surface homogeneously. The large pores, having originated from the vascular bundles of the plant biomass, are considered to be important for improving the soil quality since they can provide habitats for microorganisms. They can also act as release routes of pyrolytic vapours generated in the process of pyrolysis. Bamboo-based biochar displays good performance as a sorbent for elements, which can be further improved by physical or chemical activation processes [17].

The biochar surfaces covered with Mg (Fig. 4) and Fe (Fig. 5) particles were further investigated by the EDX analysis. EDX spectra confirmed that the nanoparticles (nanoflakes) on the surface were mainly composed of magnesium, iron and oxygen, a chemical composition that characterizes the engineered Mg-biochar (Fig. 4) and engineered Fe-biochar (Fig. 5) well. The elevated content of Cl was caused by the usage of $FeCl_3$ and $MgCl_2$ as pre-treatment solutions for feedstock preparation. On the basis of the EDX analysis, it is possible to roughly estimate the chemical composition of the samples (at the area of inspection). The molar ratio of Mg and O (2.6:2.2) in BC-B indicates that Mg is present mostly as magnesium oxide, MgO. In the case of BC-C, Fe is obviously distributed into several species. From the known thermal decomposition pathway of $FeCl_3$ [36,37], it is possible for us to suggest that the main components are Fe_2O_3 (major species), FeOOH, and FeOCl.

Both images of the surface, the EDX spectrum, as well as the SEM spectrum proved surface biochar modification. The SEM analysis of the prepared materials showed the existence of particles on the surfaces of BC-B and BC-C contrary to BC-A. SEM-EDX demonstrated the existence of Mg-particles on the surface of BC-B and Fe-particles on the surface of BC-C.

3.1.4. Thermogravimetric (TG) analysis

The thermal decomposition of the unmodified biochar BC-A and of the engineered biochars BC-B and BC-C was studied by TG analysis and is shown in Fig. 6. Upon heating, all materials released some surface water below 100°C. The unmodified biochar BC-A was then slowly pyrolyzed and this process accelerated above ~400°C. The total weight loss of 20% may be ascribed to the loss of sorbed surface water molecules, due to the decomposition of oxygen functional groups and disintegration of the carbon skeleton [38]. The second step of thermal decomposition of the engineered Mg-biochar BC-B was represented by a sharp and well-defined change in the TG curve, which was accompanied by a strong exothermic process in the DTA curve (not shown). We can assume that this process represents the decomposition of the biochar functional groups, similarly to BC-A, as well as additional calcination of the sample, which may contain some unreacted MgO precursor such as $MgCl_2$ or Mg(OH)Cl [39,40]. The engineered biochars BC-B and BC-C still contained traces of chlorides (Figs. 4 and 5) even after combustion at 460°C, as was confirmed by SEM–EDX analysis. The engineered Fe-biochar BC-C decomposed very evenly throughout the entire temperature range making it impossible to distinguish between degradation of the biochar component and calcination of residual iron chlorides. Both composites displayed significantly lower thermal stability in comparison to pure biochar compared to their composite with the clay mineral montmorillonite [41–43].

3.1.5. Fourier transform infrared spectroscopy

The FTIR spectra of the biochars BC-A, BC-B, and BC-C are shown in Fig. 7. The most intensive bands may be assigned to the stretching vibrations of aromatic C=C groups (1,585 cm^{-1}), C–O groups (broad bands in the region of ~1,160 cm^{-1}) and aromatic C–H groups (870, 808, 752, 742, and 714 cm^{-1}). In the engineered biochars BC-B and BC-C, the structure of the initial biochar BC-A had obviously collapsed. Neither bands of organic functional groups nor bands assignable to the M-O vibrations of the oxides were detectable. The lack of metal oxide vibrations is probably due to the high dilution of the sample.

3.2. Sorption experiments

Fig. 8 shows the removal efficiencies for NO_3^- and NH_4^+ from aqueous solutions of all investigated biochar samples (BC-A, BC-B, and BC-C). The sorption characteristics for NO_3^- and for NH_4^+ removal by biochar samples BC-A, BC-B, and BC-C are detailed in Table 3. The sorption capacity of the investigated sorbents increased with the increase of initial concentration of sorbate.

The engineered biochars BC-B and BC-C were more efficient for NO_3^- removal in comparison with the unmodified biochar sample BC-A (Fig. 8). The maximum sorption capacity of modified samples decreased in the order BC-C (Q_e = 10.35 mg g^{-1}), BC-B (Q_e = 9.13 mg g^{-1}), and the lowest capacity for NO_3^- removal was found in the unmodified biochar BC-A (Q_e = 4.41 mg g^{-1}). Typically, the surface of most unmodified carbon-based materials is negatively charged [7]. This characteristic limits biochar's ability for removal of anionic contaminants. In the case of samples BC-B and BC-C, however, the sorption capacity increased significantly by introduction of the Mg and Fe species.
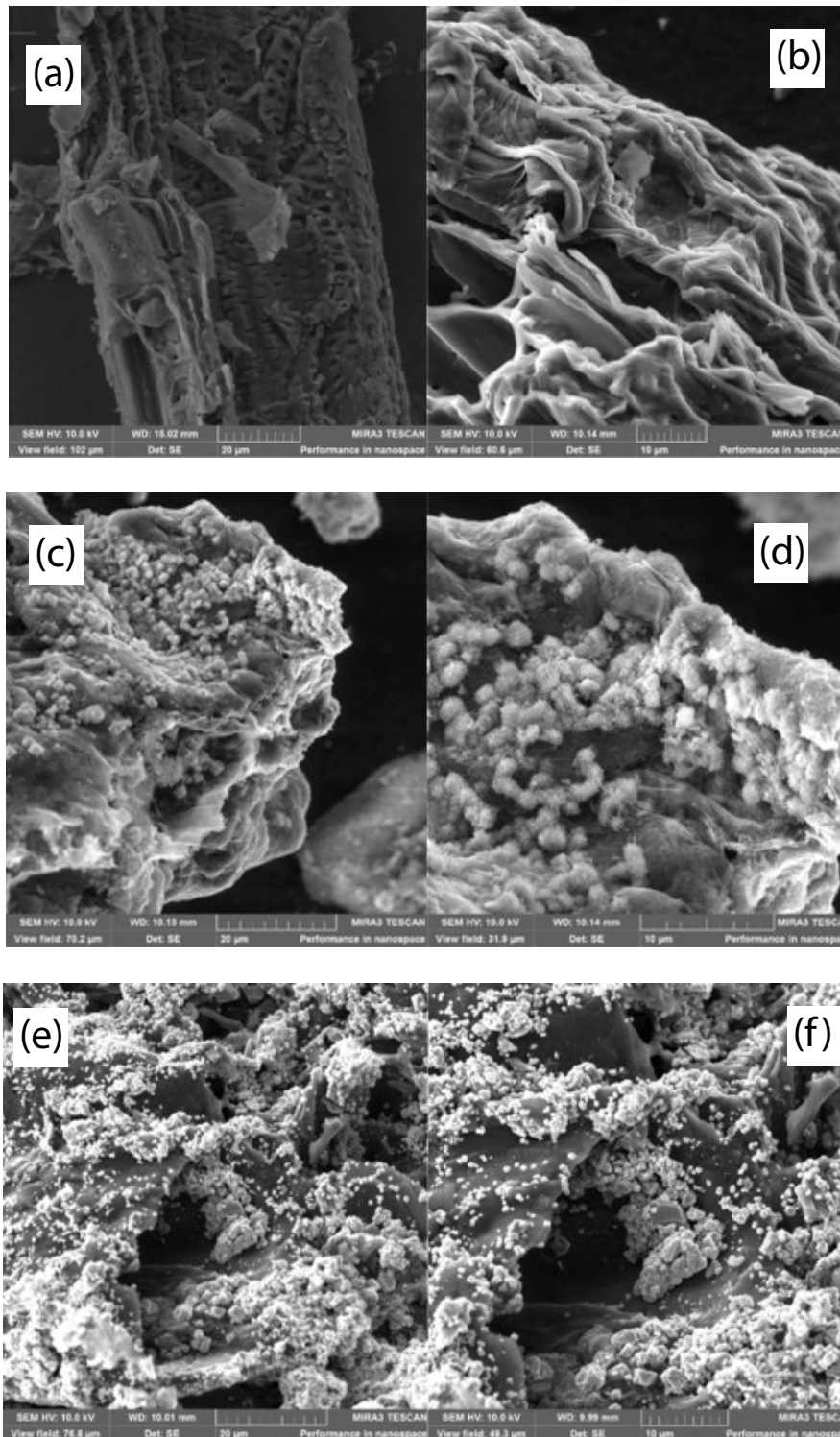
Fig. 3. Morphology of unmodified biochar (a and b), engineered Mg-biochar (c and d), and engineered Fe-biochar (e and f).

As for the NH_4^+ removal, the BC-A unmodified biochar was more efficient in comparison to the engineered biochars BC-B and BC-C. The maximum sorption capacity of the biochar samples decreased in the order BC-A (Q_e = 12.60 mg g^{-1}), BC-C (Q_e = 5.66 mg g^{-1}) and the lowest capacity for NH_4^+ removal was observed in the engineered Mg-biochar BC-B (Q_e = 3.23 mg g^{-1}). Evidently, this is also influenced by the fact that the sample BC-B forms an alkaline solution upon mixing in water, and thus a significant portion of NH_4^+ is converted into NH_3.
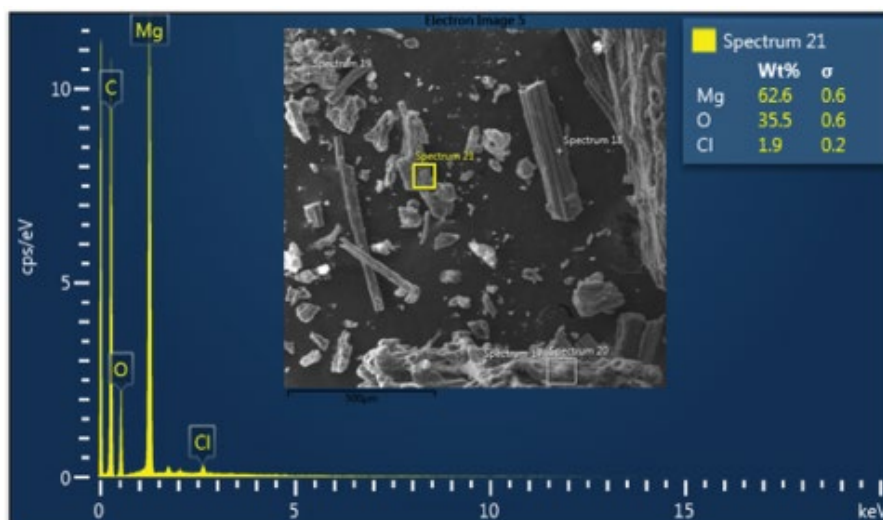
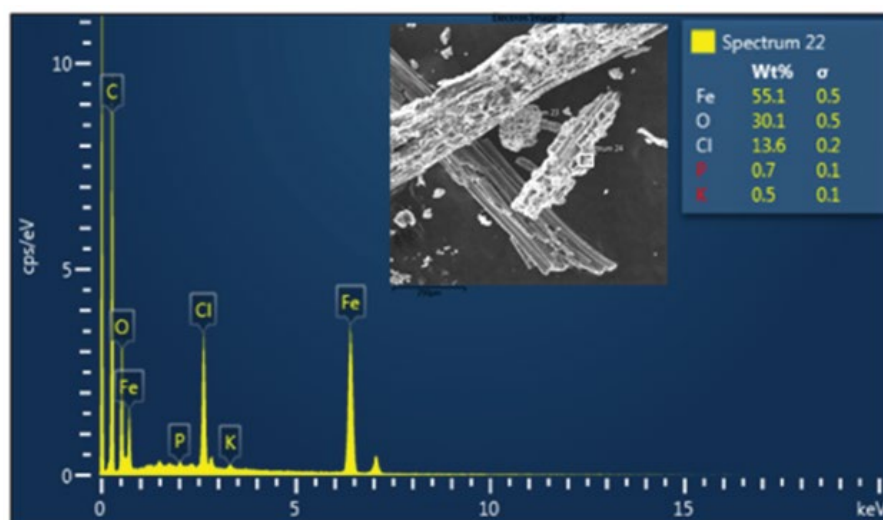Fig. 4. EDX spectrum of engineered Mg-biochar (BC-B).

Fig. 5. EDX spectrum of engineered Fe-biochar (BC-C).

The experimental data of the sorption experiments with the biochars BC-A, BC-B, and BC-C for both contaminants NH_4^+ and NO_3^- were modeled by the three most commonly used isotherms Langmuir, Freundlich, and Dubinin–Radushkevich. The Langmuir isotherm corresponded with the experimental data best in both cases, for NO_3^- and NH_4^+ removal by all three biochar samples, based on the regression coefficient (R^2). In addition, the calculated maximum sorption capacities from Langmuir isotherm for biochar samples corresponded with the experimental values for NO_3^-:BC-A Q_{exp} = 4.41 mg g^{-1} and Q_{cal} = 4.60 mg g^{-1}; BC-B Q_{exp} = 9.13 mg g^{-1}, and Q_{cal} = 10.15 mg g^{-1}; BC-C Q_e = 10.35 mg g^{-1}, and Q_{cal} = 12.85 mg g^{-1}. The experimental and calculated values of the maximum sorption capacities for NH_4^+ BC-A Q_{exp} = 12.60 mg g^{-1} and Q_{cal} = 13.78 mg g^{-1}; BC-B Q_e = 3.23 mg g^{-1}, and Q_{cal} = 3.20 mg g^{-1}; BC-B Q_e = 5.66 mg g^{-1}, and Q_{cal} = 6.17 mg g^{-1}.

The Langmuir isotherm is mainly used for cases when the sorption mechanism is only limited to a monolayer formation between the sorbent and sorbate by the total number of identical active sites, which are present on the sorbent's surface. However, this model has some limitations, such as the assumption of uniform sorption energies on the sorbent surface and the lack of interactions of sorbates on the same plane of the sorbent surface [19,44].

The data from sorption kinetics showed a rapid uptake of NH_4^+ (Fig. 10) onto BC-A unmodified biochar in the initial 60 min followed by a slower increase of uptake and equilibrium. The engineered biochars BC-B and BC-C were not so efficient for NH_4^+ removal from aqueous solutions, on the other hand, BC-A was not a good sorbent for NO_3^- (Fig. 9) removal. Just like in the case of NH_4^+, the data from sorption kinetics showed a rapid uptake of NO_3^- onto BC-B and BC-C engineered biochars within 60 min, followed

by a slower increase of uptake until equilibrium was established.

The pseudo-first and pseudo-second-order kinetics model were applied to simulate the sorption kinetics of NO_3^- and NH_4^+ to the investigated sorbents (Figs. 9 and 10). These models describe the kinetics of the solid-solution system based on mononuclear and binuclear sorption respectively, with respect to the sorbent capacity. The pseudo-second-order suited these data better, and the results are shown in Table 4. The sorption process is better described by the pseudo-second-order equation, indicating that sorption involved a chemical reaction in addition to physical sorption. Pseudo-second-order kinetic model and Langmuir isotherm model proved the best fit for the experimental adsorption data via N-pollutants removal by modified biochar, also in the investigation of other scientist [45,46].

The ability of biochar to sorb various pollutants from water and its capacity is usually lower compared to other conventional sorbents, or even biomaterials such as activated carbon. Therefore, recent studies have modified biochar to enhance its metal sorption capacity [1–3,7–10].
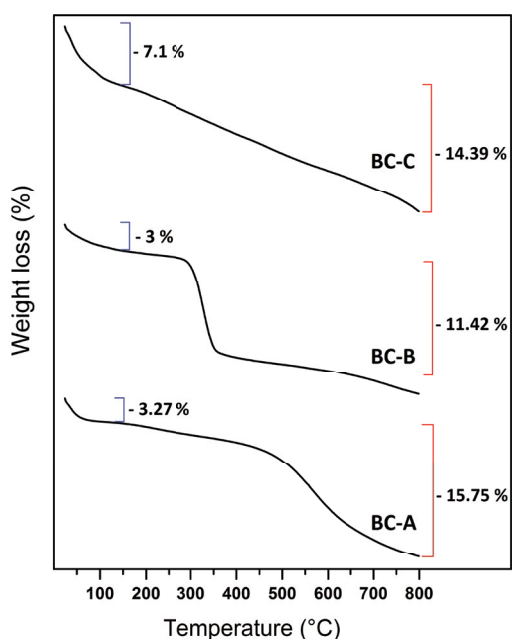

Fig. 6. Thermogravimetric spectra of biochars: engineered Fe-biochar (BC-C), engineered Mg-biochar (BC-B), and unmodified biochar BC-A. The weight losses are shown in wt.%.
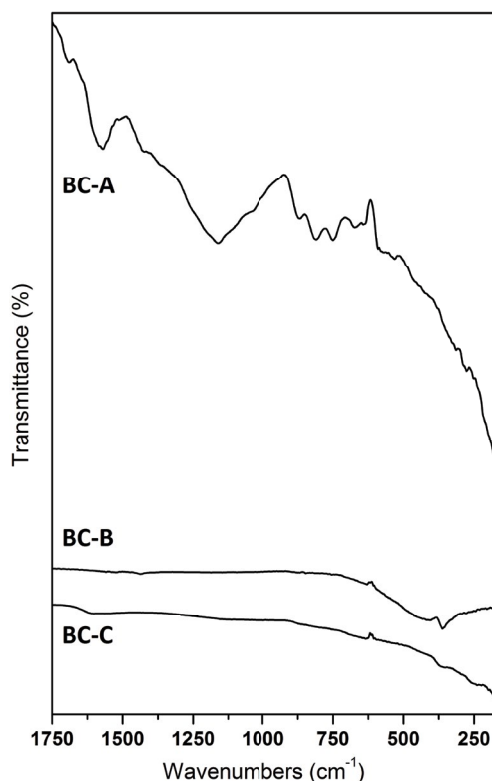

Fig. 7. FTIR spectra of biochars: unmodified biochar BC-A, engineered Mg-biochar (BC-B), and engineered Fe-biochar (BC-C).
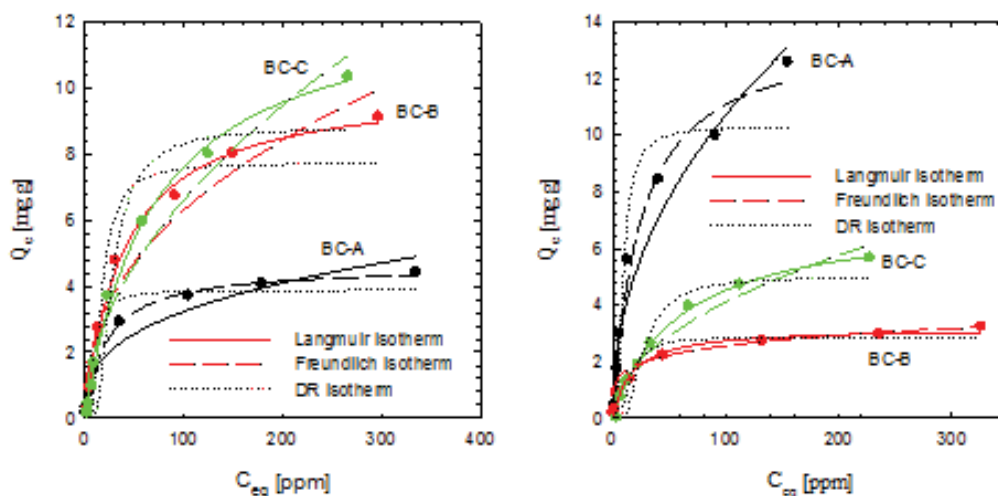

Fig. 8. Sorption isotherms of biochar samples BC-A, BC-B, and BC-C for NO_3^- (left) and for NH_4^+ (right) removal.

Table 3
Sorption isotherm characteristics for NO_3^- and for NH_4^- removal

Samples	Freundlich			Langmuir			D-R		
	K_F	n	R^2	Q_0	b	R^2	q_S	K_{AD}	R^2
BC-A NO_2^-	0.6727	0.3411	0.9368	4.6054	0.0460	0.9988	3.8826	0.0436	0.9327
BC-B NO_2^-	0.9191	0.4184	0.9499	10.1499	0.0256	0.9960	7.7386	0.0900	0.9103
BC-C NO_2^-	0.6080	0.5185	0.9690	12.8483	0.0146	0.9948	8.8175	0.2311	0.9099
BC-A NH_4^+	1.2921	0.4595	0.9471	13.78	0.0411	0.9828	10.3054	0.0288	0.9198
BC-B NH_4^+	1.0370	0.1964	0.8788	3.1967	0.0590	0.9787	2.8780	0.0766	0.8804
BC-C NH_4^+	0.4249	0.4922	0.9471	6.1699	0.0172	0.9940	5.0177	0.2269	0.8954

Table 4
Pseudo-second-order kinetics model of BC-A, BC-B, and BC-C biochars

		R^2	q_e	k_0	k_2
NH_4^+	BC-A	1	7.82	4.05	0.06626
	BC-B	0.9999	4	1.06	0.06643
	BC-C	0.9997	2.7	0.85	0.01172
NO_3^-	BC-A	0.9943	4.74	4.75	0.21134
	BC-B	1	8.01	19.76	0.30802
	BC-C	1	8.11	38.76	0.58930

The pre-treatment of biomass feedstock for the engineered biochars preparation resulted changes in their surface properties, such as the specific surface area, surface charge, functional groups, etc. [7]. However, the modification of BC-A biochar to BC-B or BC-C caused a decrease of its sorption capacity for NH_4^+, whereas the potential for NO_3^- removal has been improved significantly.

Carbon-based sorbents in a powdered form are difficult to separate from the aqueous matrix, thereby complicating the application for separation technologies [7,19]. Therefore, several methods have been established in order to produce sorbents with magnetic properties for the facilitation of efficient particle separation after the treatment process [2,20,34,43,45,47]. The engineered Fe-biochar BC-C (Fe-biochar) displayed good magnetic properties, facilitating the attraction to a permanent magnet as shown in Fig. 11. Biochar modified with Fe (BC-C) was considered to be suitable in the wastewater treatment process for N-pollutants removal. However, further research on new materials that can maintain the high magnetic properties of the biochar while preventing the deterioration of its heavy metal adsorption power is also required in the future. Moreover, studies concerning the regeneration and reuse of the utilized magnetic biochar should be conducted [19].

However, some of the disadvantages of adsorption are the high cost of conventional adsorbents, such as widely used activated carbon, adsorption capacity deterioration with the increase of cycle numbers, tedious, and time-consuming conventional separation methods for the separation of adsorbent from aqueous solution and the fact that spent adsorbent can often be considered as hazardous waste. Development of inexpensive but efficient adsorbents originating from various waste materials could be a promising alternative [46,48,49].

4. Summaries

The results of this investigation proved that modification of low-cost materials such as biochar, originating from bio-waste were successfully performed as promising adsorbents for N-pollutants removals from aqueous media. The main objective of this research was to prove the sorption properties of Fe-Mg-modified biochar toward the nitrogen pollutant, in order to enhance its application for ground and waste-water treatment. After the identification of bamboo (*P. viridiglaucescens*) as a suitable, easily obtainable and inexpensive biomass, raw biochar was produced in a pyrolysis reactor with a nitrogen atmosphere. Chemical modification was used as a pre-treatment method for the novel engineered biochars, containing the species of Mg and Fe in the form of nano-sized particles on biochar's porous surface, which were proved in several ways. The prepared samples of biochar can successfully remove nitrates and to some extent, ammonium from aqueous solutions as well. The results showed that the sorption equilibrium was obtained after 60 min. The experimental data corresponded well to the pseudo-second-order kinetic model and the Langmuir isotherm model. The maximum sorption capacity of raw bamboo biochar was 4.41 (mg g^{-1}) for ammonium. For the anionic nitrate, the maximum sorption capacities of the engineered biochars were 9.13 (mg g^{-1}) for the engineered Mg-biochar and 10.35 (mg g^{-1}) for the engineered Fe-biochar. The engineered Fe-biochar displayed good magnetic properties, facilitating the attraction to a permanent magnet.

Conflict of interest statement

We have no conflicts of interest to disclose and the manuscript is a work of us; the manuscript has been approved by all co-authors.
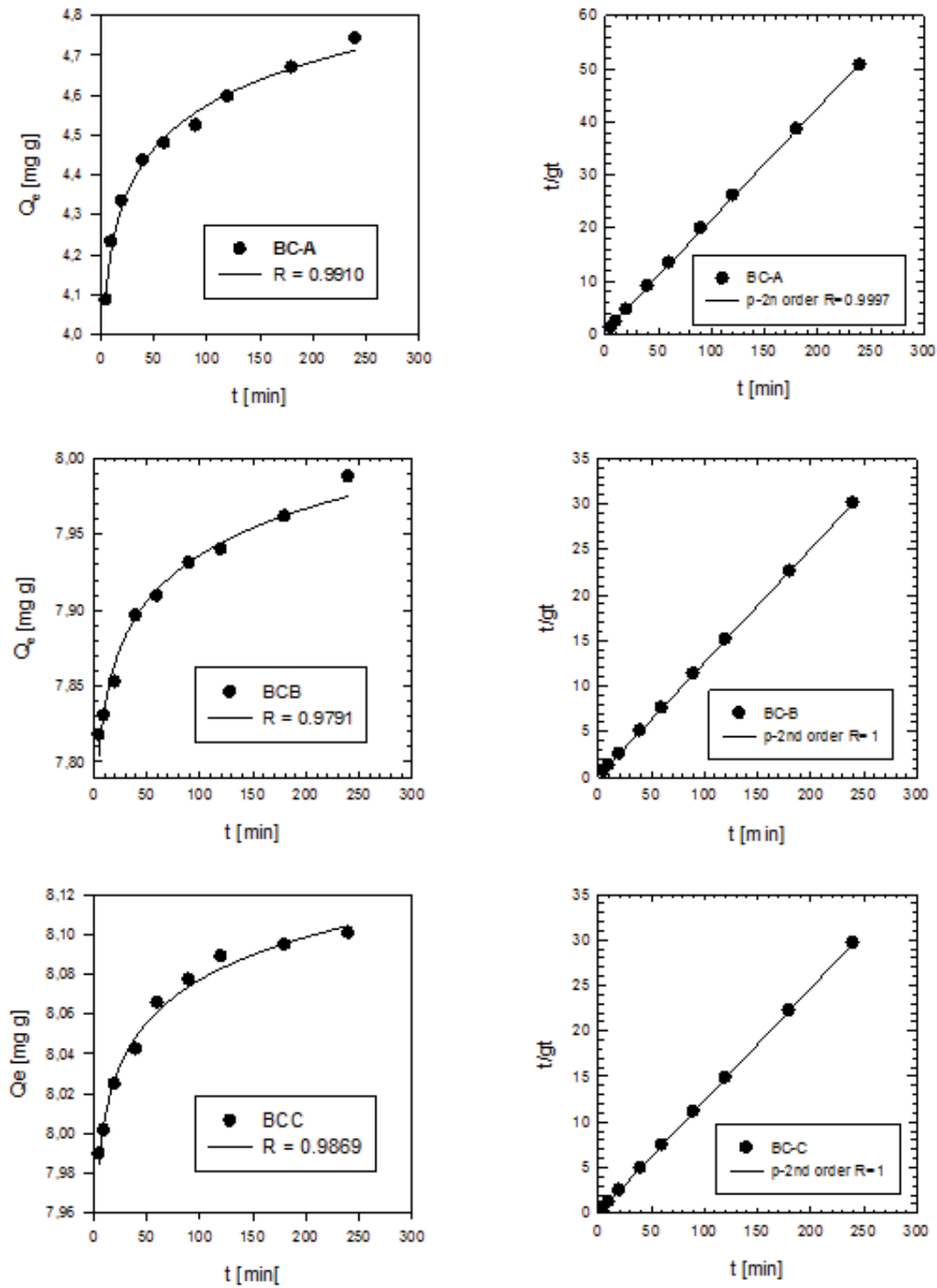
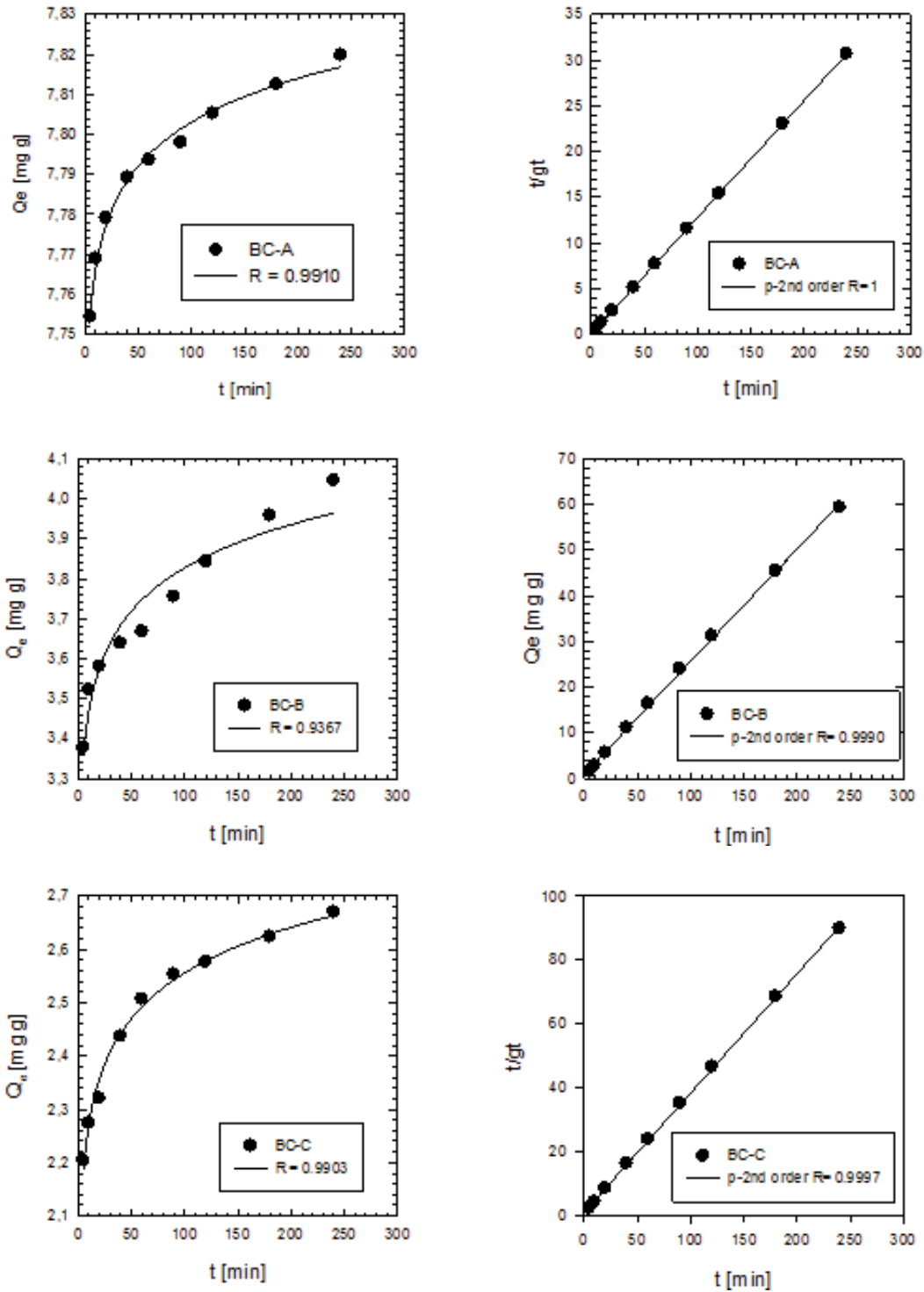Fig. 9. Influence of contact time and pseudo-second kinetics order for NO_3^- sorption.

Fig. 10. Influence of contact time and pseudo-second kinetics order for NH_4^- sorption.

V_{micro} —   Volume of micropore
V_{tot} —   Volume of total pore volume
ε —   DR isotherm constant

Fig. 11. The engineered Fe-biochar sample (BC-C), showing magnetic properties by attraction to the permanent magnet.

Symbols

b —   Sorption ratio of sorption/desorption rates
C_0 —   Initial concentration
C_{eq} —   Equilibrium concentration
C_S —   Sorption capacity (Langmuir isotherm)
$C_{S\text{max}}$ —   Maximum of sorption capacity/site saturation
K_{ad} —   DR isotherm constant
K_F —   Freundlich isotherm constant
Q_e —   Sorption capacity (calculations)
q_s —   Theoretical isotherm saturation capacity
S_{BET} —   Specific surface area
S_T —   External surface area
V —   Volume of an aqueous solution

References

[1]   A. Bhatnagar, M. Sillanpää, A review of emerging adsorbents for nitrate removal from water, Chem. Eng. J., 168 (2011) 493–504.

[2]   B. Chen, Z. Chen, S. Lv, A novel magnetic biochar efficiently sorbs organic pollutants and phosphates, Bioresour. Technol., 102 (2011) 716–723.

[3]   P. Loganathan, S. Vigneswaran, J. Kandasamy, Enhanced removal of nitrate from water using surface modification of adsorbents –a review, J. Environ. Manage., 131 (2013) 363–374.

[4]   O. Pastushok, F. Zhao, D.L. Ramasamy, M. Sillanpää, Nitrate removal and recovery by capacitive deionization (CDI), Chem. Eng. J., 375 (2019) 121943.

[5]   C.V. Lazaratou, D.V. Vayenas, D. Papoulis, The role of clays, clay minerals and clay-based materials for nitrate removal from water systems: a review, Appl. Clay. Sci., 185 (2020) 105377.

[6]   M. Shrimali, K.P. Singh, New methods of nitrate removal from water, Environ. Pollut., 112 (2001) 351–359.

[7]   H. Li, X. Dong, E.B. da Silva, L.M. de Oliviera, Y. Chen, L.Q. Ma, Mechanisms of metal sorption by biochars: biochar characteristics and modifications, Chemosphere, 178 (2017) 466–478.

[8]   D. Mohan, P. Singh, A. Sarswat, P.H. Steele, C.U. Pittman Jr., Lead sorptive removal using magnetic and nonmagnetic fast pyrolysis energy cane biochars, J. Colloid Interface Sci., 448 (2015) 238–250.

[9]   X. Tan, Y. Liu, G. Zeng, X. Wang, X. Hu, Y. Gu, Z. Yang, Application of biochar for the removal of pollutants from aqueous solutions, Chemosphere, 125 (2015) 70–85.

[10] K.R. Thinnes, E.C. Abdullah, N.M. Mubarak, M. Ruthiraan, Synthesis of magnetic biochar from agricultural waste biomass to enhancing route for waste-water polymer application: a review, Renewable Sustainable Energy Rev., 67 (2017) 257–276.

[11] A.U. Rajapaksha, S.S. Chen, D.C.W. Tsang, M. Zhang, M. Vithanage, S. Mandal, B. Gao, N.S. Bolan, Y.S. Ok, Engineered/ designer biochar for contaminant removal/immobilization from soil and water: potential and implication of biochar modification, Chemosphere, 148 (2016) 276–291.

[12] A. El-Naggar, S.S. Lee, J. Rinklebe, M. Farooq, H. Song, A.K. Sarmah, A.R. Zimmerman, M. Ahmad, S.M. Shaheen, Y.S. Ok, Biochar application to low fertility soils: a review of current status, and future prospects, Geoderma, 337 (2019) 536–554.

[13] A. El-Naggar, A.H. El-Naggar, S.M. Shaheen, B. Sarkar, S.X. Chang, D.C.W. Tsang, J. Rinklebe, Y.S. Ok, Biochar composition-dependent impacts on soul nutrient release, carbon mineralization, and potential environmental risk: a review, J. Environ. Manage., 241 (2019) 458–467.

[14] M.B. Khan, X. Cui, G. Jilani, L. Tang, M. Lu, X. Cao, Z.A. Sahito, Y. Hamid, B. Hussain, X. Yang, Z. He, New insight into the impact of biochar during vermi-stabilazation of divergent biowastes: literature synthesis and research pursuits, Chemosphere, 238 (2020) 1246–1279.

[15] X, Gong, L. Cai, S. Li, S.X. Chang, X. Sun, Z. An, Bamboo biochar amendment improves the growth and reproduction of *Eisenia fetida* and the quality of green waste vermicompost, Ecotoxicol. Environ. Saf., 156 (2019) 197–204.

[16] J. Lehmann, S. Joseph, Biochar for Environmental Management: Science and Technology, Earthscan Press, 2009, p. 332.

[17] L. Hernandéz-Mena, A. Pecora, A. Beraldo, Slow pyrolysis of bamboo biomas: analysis of biochar properties, Chem. Eng. Trans., 37 (2014) 115–120.

[18] J. Jin, S. Li, X. Peng, W. Liu, C. Zhang, Y. Yang, L. Han, Z. Du, K. Sun, X. Wang, HNO₃ modified biochars for uranium(VI) removal from aqueous solution, Bioresour. Technol., 55 (2018) 567–572.

[19] H.P. Lu, Z.A. Li, G. Gascó, A. Méndez, Y. Shen, J. Paz-Ferreiro, Use of magnetic biochars for the immobilization of heavy

metals in a multi-contaminated soil, Sci. Total Environ., 622–623 (2018) 892–899.

[20] E.B. Son, K.M. Poo, J.S. Chang, K.J. Chae, Heavy metal removal from aqueous solutions using engineered magnetic biochars derived from waste marine macro-algal biomass, Sci. Total Environ., 615 (2018) 161–168.

[21] L. Beesley, M. Marmiroli, The immobilisation and retention of soluble arsenic, cadmium and zinc by biochar, Environ. Pollut., 159 (2011) 474–480.

[22] A. Mukherjee, A.R. Zimmerman, W. Harris, Surface chemistry variations among a series of laboratory-produced biochars, Geoderma, 163 (2011) 247–255.

[23] M. Mazarji, B. Aminzadeh, M. Baghdadi, A. Bhantnagar, Removal of nitrate from aqueous solution using modified granular activated carbon, J. Mol. Liq., 233 (2017) 139–148.

[24] M. Thommes, K. Kaneko, A.V. Neimark, J.P. Olivier, F. Rodriguez-Reinoso, J. Rouquerol, K.S.W. Sing, Physisorption of gases, with special reference to the evaluation of surface area and pore size distribution (IUPAC Technical Report), Pure Appl. Chem., 87 (2015) 1051–1069.

[25] J.D. Boer, B. Lippens, B. Linsen, J. Broekhoff, A.V.D. Heuvel, T.J. Osinga, The t-curve of multimolecular N_2-adsorption, J. Colloid Interface Sci., 21 (1966) 405–414.

[26] E.P. Barrett, L.G. Joyner, P.P. Halenda, The determination of pore volume and area distributions in porous substances. I. Computations from nitrogen isotherms, J. Am. Chem. Soc., 73 (1951) 373–380.

[27] I. Langmuir, The constitution and fundamental properties of solids and liquids, J. Am. Chem. Soc., 38 (1916) 2221–2295.

[28] H.M.F. Freundlich, Over the adsorption in solution, J. Phys. Chem., 57 (1906) 385–471.

[29] A. Günay, E. Arslankaya, İ. Tosun, Lead removal from aqueous solution by natural and pretreated clinoptilolite: adsorption equilibrium and kinetics, J. Hazard. Mater., 146 (2007) 362–371.

[30] M.M. Dubinin, L.V. Radushkievich, The equation of the characteristic of the activated charcoal, Proc Acad Sci. Phys. Chem. Sect., 55 (1947) 331–337.

[31] S. Lagergren, Zur theorie der sogenannten adsorption geloster stoffe, Kungl. Svenska Vetenskapsakad., 24 (1989) 1–39.

[32] Y.S. Ho, G. McKay, Pseudo-second-order model for sorption processes, Process Biochem., 34 (1999) 451–465.

[33] H. Sun, W.C. Hockaday, C.A. Masiello, K. Zygourakis, Multiple controls on the chemical and physical structure of biochars, Ind. Eng. Chem. Res., 51 (2012) 3587–3597.

[34] D. Mohan, A. Sarswat, Y.S. Ok, C.U. Pittman Jr., Organic and inorganic contaminants removal from water with biochar, renewable, low cost sustainable adsorbent – a critical review, Bioresour. Technol., 160 (2014) 191–202.

[35] P. Hudec, Textúra Tuhých Látok. Charakterizácia Adsorbentov a Katalyzátorov Fyzikálnou Adsorpciou Dusíka, Slovak Technical University, Slovakia, 2012, p. 311.

[36] L. Chen, X.L. Chen, C.H. Zhou, H.M. Yang, S.F. Ji, D.S. Tong, Z.K. Zhong, W.H. Yu, M.Q. Chu, Environmental-friendly montmorillonite-biochar composites: facile production and tunable adsorption-release of ammonium and phosphate, J. Cleaner Prod., 156 (2017) 648–659.

[37] S.B. Kanungo, S.K. Mishra, Thermal dehydratation and decomposition of $FeCl_3 \cdot xH_2O$, J. Therm. Anal., 46 (1996) 1487–1500.

[38] M. Zhang, B. Gao, Y. Yao, Y. Xue, M. Inyang, Synthesis, characterization, and environmental implications of graphene-coated biochar, Sci. Total Environ., 435–436 (2012) 567–572.

[39] Q. Huang, G. Lu, J. Wang, J. Yu, Thermal decomposition mechanism of $MgCl_2 \cdot 6H_2O$ and $MgCl_2 \cdot H_2O$, J. Anal. Appl. Pyrolysis, 91 (2011) 159–164.

[40] M. Zhang, B. Gao, Y. Yao, Y. Xue, M. Inyang, Synthesis of porous MgO-biochar nanocomposites for removal of phosphate and nitrate from aqueous solution, Chem. Eng. J., 210 (2012) 26–32.

[41] E. Viglašová, M. Galamboš, Z. Danková, L. Krivosudský, C.L. Lengauer, R. Hood-Nowotny, G. Soja, A. Rompel, M. Matík, J. Briančin, Production, characterization and adsorption studies of bamboo-based biochar/montmorillonite composite for nitrate removal, Waste Manage., 79 (2018) 385–394.

[42] C. Beusch, A. Cierjacks, J. Böhn, J. Martens, W.-A. Bischoff, J.C. de Araújo Filho, M. Kaupenjohann, Biochar vs. clays: comparison of their effects on nutrient retention of a tropical arenosol, Geoderma, 337 (2019) 524–535.

[43] R. Tareq, N. Akter, Md.S. Azam, Chapter 10: Biochars and Biochar Composites: Low-Cost Adsorbents for Environmental Remediation, Biochar from Biomass and Waste Fundamentals and Applications, Elsevier, 2019, pp. 169–209.

[44] M. Ghasemi, M. Naushad, N. Ghasemi, Y. Khosravi-Fard, Adsorption of Pb(II) from aqueous solution using new adsorbents prepared from agricultural waste: adsorption and kinetic studies, J. Ind. Eng. Chem., 20 (2014) 2193–2199.

[45] R.B. Fidel, D.A. Laird, K.A. Spokas, Sorption of ammonium and nitrate to biochars is electrostatic and pH-dependent, Sci. Rep., 8 (2018) 17627.

[46] L.D. Hafshejani, A. Hooshmand, A.A. Naseri, A.S. Mohammadi, F. Abbasi, A. Bhatnagar, Removal of nitrate from aqueous solution by modified sugarcane bagasse biochar, Ecol. Eng., 95 (2016) 101–111.

[47] E. Agrafioti, D. Kalderis, E. Diamadopoulos, Ca and Fe modified biochars as adsorbents of arsenic and chromium in aqueous solutions, J. Environ. Manage., 146 (2014) 444–450.

[48] A. Rahmani, H.Z. Mousavi, M. Fazli, Effect of nanostructure alumina on adsorption of heavy metals, Desalination, 253 (2010) 94–100.

[49] M. Stjepanović, N. Velić, A. Lončarić, D. Gašo-Sokač, V. Bušić, M. Habuda-Stanić, Adsorptive removal of nitrate from wastewater using modified lignocellulosic waste material, J. Mol. Liq., 285 (2019) 535–544.